

MIT Open Access Articles

*Hyperstage Graphite: Electrochemical
Synthesis and Spontaneous Reactive Exfoliation*

The MIT Faculty has made this article openly available. **Please share**
how this access benefits you. Your story matters.

Citation: Jeon, Intak, et al. "Hyperstage Graphite: Electrochemical Synthesis and Spontaneous Reactive Exfoliation." *Advanced Materials*, vol. 30, no. 3, Jan. 2018, p. 1704538.

As Published: <http://dx.doi.org/10.1002/adma.201704538>

Publisher: Wiley Blackwell

Persistent URL: <http://hdl.handle.net/1721.1/114414>

Version: Author's final manuscript: final author's manuscript post peer review, without publisher's formatting or copy editing

Terms of use: Creative Commons Attribution-Noncommercial-Share Alike



DOI: 10.1002/((please add manuscript number))

Article type: Communication

Hyperstage Graphite: Electrochemical Synthesis and Spontaneous Reactive Exfoliation

*Intak Jeon, Bora Yoon, Maggie He, and Timothy M. Swager**

I. Jeon

Department of Materials Science and Engineering, Institute for Soldier Nanotechnologies
Massachusetts Institute of Technology
Cambridge, Massachusetts 02139, USA

B. Yoon, M. He, and T. M. Swager

Department of Chemistry, Institute for Soldier Nanotechnologies
Massachusetts Institute of Technology
Cambridge, Massachusetts 02139, USA
E-mail: tswager@mit.edu

Keywords: Hyperstage-1 graphite intercalation compound, spontaneous exfoliation, functionalized graphene, diazonium salt, Meisenheimer complex

Abstract

Covalent modification of the π -electron basal planes of graphene enables the formation of new materials with enhanced functionality. We report an electrochemical method for the formation of what we refer to as a Hyperstage-1 graphite intercalation compound (GIC), which has a very large interlayer spacing $d_{001} > 15.3 \text{ \AA}$ and contains disordered interstitial molecules/ions. This material is highly activated and undergoes spontaneous exfoliation when reacted with diazonium ions to produce soluble graphenes with high functionalization densities of one pendant aromatic ring for every 12 graphene carbons. Critical to achieving high functionalization density is the Hyperstage-1 GIC state, are a weakening of the van der Waals coupling between adjacent graphene layers, and the ability of reactants to diffuse into the disordered intercalate phase between the layers. Graphene functionalization with 3,5-dinitrophenyl (3,5-DiNP) groups, provides for exceptional dispersibility (0.24 mg ml^{-1}) in *N,N*-dimethylformamide (DMF) and for conjugation with amines.

Main

Advances in graphene science and technology depend critically on manipulating new forms of graphene into functional materials. Chemical methods are attractive because they can tailor the physical, electronic, mechanical, thermal, and/or transport properties of graphenes for a specific applications.^[1-4] Many functionalization schemes take advantage of defect sites and oxygen groups on graphene oxide (GO) or reduced graphene oxide (rGO).^[5-7] However, the highly degraded carbon framework of GO and rGO ultimately limit the performance of these materials. Therefore, efficient methods for the bulk production of high quality functionalized graphenes are needed. Graphite can be activated by reducing the intersheet van der Waals attractions by inserting atomic or molecular layers of alkali metals, acids or FeCl₃, between the graphene sheets. Despite the application of harsh chemical and thermal conditions, only partial GICs are typically produced in these methods.^[8-10] Proper analysis of these processes requires rigorous studies of the crystal structure of GICs. Although the use of GICs as activated intermediates in chemical functionalization has enjoyed success, typical exfoliation schemes require prolonged high power ultrasonication, which degrades the graphene.^[11-13] Additionally, the resulting graphene dispersions are often meta-stable and re-aggregation generally occurs.^[14, 15]

We demonstrate herein, a gentle room temperature (RT) method for reducing the van der Waals coupling between graphene sheets ($d_{001} > 15.3 \text{ \AA}$) and subsequent spontaneous exfoliation to give soluble functionalized graphene. This is not the first demonstration of electrochemical activation and functionalization of graphene, however previous investigations,^[16] including those from our own group, failed to quantitatively produce pure isolated sheets, giving instead inseparable mixtures that contain some multilayer graphenes. Our methods involves the intercalation of tetrabutylammonium (TBA⁺) into the graphene galleries which electrostatically balance the negatively charged π -electron system created electrochemically. Increased d_{001} -spacing in Stage-1 GIC reduces van der Waals interactions

1
2
3
4
5
6
7
8
9
10
11
12
13
14
15
16
17
18
19
20
21
22
23
24
25
26
27
28
29
30
31
32
33
34
35
36
37
38
39
40
41
42
43
44
45
46
47
48
49
50
51
52
53
54
55
56
57
58
59
60
61
62
63
64
65

between graphenes. However, as we describe, the crystalline organization of the TBA⁺ ions,^[17] restricts reactant diffusion into the network and thereby reduces reactivity. At high negative potentials, it is possible to both increase the intercalation of large density of TBA⁺ ions and introduce amines by electrolytic decomposition of the TBA⁺. The result is a further expanded gallery with a disordered interstitial phase between the basal planes to give what we refer to as a Hyperstage-1 GICs. The result has great utility because every graphene layer is accessible to react with diazonium salts in this process the graphene spontaneously exfoliates without any deliberate mixing or sonication. The diazonium reaction of the Hyperstage-1 GIC results in exceptionally high densities of functional groups on the graphene. We further demonstrate that by functionalization with 3,5-dinitrophenyl enables the formation of Meisenheimer complexes between functionalized graphene and *n*-butylamine.

Our goal is to create extended functionalized graphenes with minimal defects in the hexagonal graphene lattice. As a result, highly oriented pyrolytic graphite (HOPG) was chosen as a high purity graphite source. In contrast to randomly oriented graphite, HOPG conserves the monolithic structure and electrical connectivity of the graphite domains throughout the necessary expansion that accompanies the electrochemical generation of the different GICs. The electrochemically driven intercalation process is depicted in **Figure 1**. In this scheme, high reducing potentials of HOPG results in TBA intercalation between the graphene sheets. The solvent is key to this process and we find that a mixture of acetonitrile (MeCN) and dimethylformamide (DMF) enhances this process over our previous procedures.^[16] A continuous electrochemical potential ramp maintains a driving force for full intercalation of TBA⁺, which is accompanied by a dramatic volumetric expansion of HOPG.

In this process we identified five voltage ranges (I, II, III, IV and V in **Figure 2**) that correspond to distinct phases of GIC staging. These include the Stage-1, Hyper-1-Stage-1, Hyper-2-Stage-1, and Hyper-3-Stage-1, which as shown in **Figure 2** have varying degrees of ion intercalation and intersheet spacing. Since the electromigration of the larger molecule

1 TBA⁺ in graphene galleries was predictably sluggish, we experimentally observed specific
2 current peaks associated with changes in staging only with extremely slow voltage sweeps
3
4
5 (−40 μV s^{−1}).
6

7 The different GIC stages were identified by X-ray diffraction (XRD), which reveals
8
9 different crystallographic lattice arrangements of intercalants and graphite layers along the c-
10 axis (**Figure 3**).^[18] As intercalation takes place, the graphite (002) peak vanishes and new
11 peaks appear. The dominant diffractions in Stage-1 GIC appeared in the (00ℓ) reflections are
12 a direct measure of the interlayer distance (d_{001} of ~8.17 Å). The introduction of the
13 intercalated layer weakens the attractive potential between graphite layers, however the
14 material is still relatively inert as result of the ordered intercalation ions. The interlayer
15 distance is in agreement with the expected size of TBA⁺ in a flattened conformation (~4.8 Å)
16 within the graphene galleries.^[19] With increasing voltage, the graphene/TBA⁺ matrix exhibits
17 an increasing d_{001} spacing (3.35 → 8.17 → 12.70 → 15.30 Å → disordered) (**Figure S1 and**
18 **S2**). The structural disorder of the intercalation phase is highest for Hyper-3-Stage-1 GIC, and
19 we attribute this to the reductive decomposition of TBA⁺ ions within graphene galleries.^[20]
20 Our hypothesis is that reductive fragmentation of TBA⁺ ions decomposes into tributylamine,
21 butene and alkanes (**Figure S3 and S4**). These fragments disrupt much of the crystalline
22 organization of the ions, which as will be discussed allow facilitate functionalization.
23 However, we still observe minor diffraction peaks that are ascribed to electrolyte.
24
25
26
27
28
29
30
31
32
33
34
35
36
37
38
39
40
41
42
43
44
45

46 The disorder in the Hyper-3-Stage-1 GIC produces greatly enhanced reactivity and
47 transferring this material as an activated electrode to a solution containing 0.1 M 3,5-
48 dinitrobenzenediazonium tetrafluoroborate (3,5-DiNBD) and 1 M TBAP in MeCN with a
49 negative potential ramp from −1.2 to −2.0 V (vs Ag/Ag⁺, −10 μV S^{−1}) resulted in efficient
50 reductive functionalization (**Figure S5**). Under these conditions we observe remarkable
51 behavior with the graphite undergoing spontaneous exfoliation to give MeCN solutions of
52
53
54
55
56
57
58
59
60
61
62
63
64
65

soluble functionalized graphene. XRD of the purified functionalized graphene revealed a completely amorphous material that lacks typical intergraphene sheet diffractions (**Figure 3**). This is unusual for a functionalized graphene and we attribute this to the high degrees of functionalization that tend to prevent the sheets from organizing into 2D structures.

Raman spectroscopy was used to characterize HOPG, Stage-1, Hyper-2-Stage-1, Hyper-3-Stage-1 GICs, exfoliated graphene and functionalized graphene (**Figure 4a**).^[21] The D and 2D-bands displayed similar shifts with TBA⁺ intercalation and, in transition from HOPG to Hyper-2-Stage-1 GICs, these peaks gradually shifted to lower frequencies (-41.1 cm^{-1} for D-band and -74.1 cm^{-1} for 2D band). This shifts are indicative of *n*-doping resulting from electrochemical reduction of the graphene with concurrent TBA⁺ intercalation (**Figure S6**).^[22] The D and 2D-bands broadened with increasing TBA⁺ density, and the G-band splits and shifts upon formation of different staged compounds (**Figure S6 and Figure S7**).^[23] The G-band depends strongly on the charge carrier densities and the observed shift to higher frequencies is consistent with recent reports on electron doping by electrochemical gating.^[24]^[25] The G-band of graphite appears at 1580 cm^{-1} and shifts to $1603.0\text{--}1605.1\text{ cm}^{-1}$ in Stage-1/Hyper-2-Stage-1-GICs, respectively (**Figure 4a and Figure S6**). The G band of Hyper-3-Stage-1 GIC also exhibits complexity with multiple overlapped peaks that can be deconvoluted into 4 distinct peaks (**Figure 4a and Figure S6**). These peaks for Hyper-3-Stage-1 GIC can be assigned to *n*-doping with TBA⁺ intercalation as well as the presence of highly undulated graphene layers.^[26-28]

We confirmed that electrochemical intercalation doesn't result in covalent functionalization of the graphene sheets by analyzing the exfoliated (ultrasonication) purified (washed) material. Specifically, we find that the intensities of the Raman I_D/I_G and I_D/I_D' bands of exfoliated graphene from Hyper-3-Stage-1 GIC are 0.3 and 2.4, respectively (**Figure 4a and Figure S8**). These exfoliated defect free graphenes readily reassemble into stacked sheets when isolated and the powders display the characteristic (002) reflection of graphite

1
2
3
4
5
6
7
8
9
10
11
12
13
14
15
16
(Figure S9). As a result, the electrochemical activation does not result in irreversible functionalization of the graphene sheets. In contrast after spontaneous exfoliation of functionalized graphene with 3,5-DiNP groups from Hyper-3-Stage-1 GIC, the Raman spectra indicate extensive covalent functionalization on the basal plane. The dramatically broadened lines of the D and G bands and the I_D/I_G ratio (~ 0.71) confirm the introduction of a high percentage of sp^3 -hybridized carbon atoms into the sp^2 -hybridized graphene (**Figure 4a and Figure S6**).

17
18
19
20
21
22
23
24
25
26
27
28
29
30
31
32
33
34
35
36
37
38
39
40
41
42
43
XPS provides additional insight into the chemical nature of the GICs and functionalized graphene. The deconvolution of the C 1s peak reveals the presence of sp^2 C–C (~ 284.5 eV), sp^3 C–C/C–OH (~ 285.5 eV), C–O/C–N⁺ (~ 286.3 eV), C=O (287.6 eV), and a shake-up peak (~ 291 eV) in **Figure 4b**.^[29, 30] The relative intensity of the different sp^3 component peaks (~ 285.5 and ~ 286.3 eV) in Stage-1, Hyper-2-Stage-1, Hyper-3-Stage-1 GICs are all consistent with the amount of intercalated TBA⁺.^[31] The analysis of the nitrogen peaks is also relevant, and Hyper-2-Stage-1 and Hyper-3-Stage-1 GICs provided a pure intercalated phase with a peak at 402.8 eV corresponding to the N 1s of the quaternary TBA⁺ (**Figure S10**). The additional N 1s peaks at 400.3 eV and 398.4 eV in Hyper-3-Stage-1 GIC are attributed to TBA⁺ reduction products and solvent molecules (MeCN and DMF) in the graphene galleries (**Figure 4c and Figure S10**).^[30, 32]

44
45
46
47
48
49
50
51
52
53
54
55
56
57
58
59
60
61
62
63
64
65
XPS of graphene functionalized with 3,5-dinitrophenyl (3,5-DiNP) after purification produced an exceptionally strong N 1s peak in the XPS spectra. The C/N ratio of ~ 8.5 reveals an extraordinarily high functionalization density of one 3,5-DiNP group per 12 carbon atoms (**Figure S6C**). A high-resolution N 1s analysis revealed three peaks centered at 398.5, 400.5 and 404.7 eV (**Figure 4d and e**).^[33-35] The major peak at higher binding energy (404.7 eV) is assigned to the nitrogen of the nitro groups, thereby confirming the presence of 3,5-DiNP groups attached to the graphene (**Figure S10 and S11**). The broad and lower binding energy N 1s peaks at 400.5 and 398.5 eV are assigned to nitrogens from reduction of the nitro groups

1 produced under the electrochemical conditions. Specifically we expect that reduction of the
2 nitro groups will give rise to Ph-NHOH and/or Ph-NH₂ units. These processes are also
3 facilitated by the H atoms that can be extracted from the solvent and the products generated
4 by the reductive decomposition of the TBA⁺ electrolyte. The XRD data reveals the reason for
5 this lack of reactivity and peaks associated with ordered TBA⁺ ions in the gallery likely
6 provide for a rigid network that blocks diffusion of other reagents into the interior of the
7 material. The introduction of amine reduction products in Hyper-3-Stage-1, confirmed by the
8 XPS N 1s peaks, produces disorder in the graphene galleries thereby allowing diazonium
9 reagents to diffuse into the galleries (**Figure 2f**).

10
11
12
13
14
15
16
17
18
19
20
21
22 The functionalized graphene sheets were investigated by transmission electron
23 microscopy (TEM) and atomic force microscopy (AFM) in order to obtain additional
24 microscopic evidence of the covalent functionalization. Exfoliated single layer graphene
25 produced by ultrasonic exfoliation of the Hyper-3-Stage 1 GIC exhibited a single set of
26 sharp peaks associated with a graphitic hexagonal diffraction pattern (**Figure 5a**). The
27 relative intensity ratio of $I_{\{1100\}}/I_{\{2110\}}$ is approximately 1.35, which is in agreement with
28 previous reports.^[36] In the case of our functionalized graphene, the surface of the graphene
29 sheets appeared to have some heterogeneity suggesting that sections are heavily covered with
30 pendant phenyl groups (**Figure 5b**) and others may have lower functionalization. In spite of
31 the functionalization, the sample still displays hexagonal crystalline domains, however these
32 are distorted with a $d_{\{1100\}} = 2.12 \sim 2.28 \text{ \AA}$ as compared to graphene with $d_{\{1100\}} = 2.13 \text{ \AA}$ as
33 determined by electron diffraction. **An average thickness of $\sim 4.3 \text{ nm}$ was observed for**
34 **functionalized graphenes according to the AFM profile (Figure 5c). Figure 5d shows a**
35 **histogram of thickness of functionalized graphene and reveals two distinct thicknesses of 2.4**
36 **and 4.4 nm. These heights correspond to two-sided functionalized single and double layer**
37 **graphene structures respectively and suggests that our method specifically produces**
38 **dominantly single/double layer exfoliations.**^[37] The double layer structures may result from
39
40
41
42
43
44
45
46
47
48
49
50
51
52
53
54
55
56
57
58
59
60
61
62
63
64
65

1 post functionalization aggregation. AFM analysis provided an average sheet area of 0.032
2 μm^2 , which is smaller than the average domain size of the precursor graphite (intraplanar
3 microcrystalline size: 1–10 μm) (**Figure 5e and Figure S12**).^[38]
4
5

6
7 We sought to take advantage of the ability of the electron-deficient 3,5-DiNP groups
8 in our functionalized graphene to form Meisenheimer complexes with *n*-butylamine. A
9 schematic illustration of Meisenheimer complex formation from 3,5-dinitrobenzene
10 functionalized graphene and *n*-butylamine is shown in **Figure 6a**. When compared with the
11 functionalized graphene with 3,5-DiNP groups, the Meisenheimer complex graphene provides
12 improved dispersion stability in MeCN (**Figure 6b**). We noticed that graphene dispersed with *n*-
13 butylamine doesn't form a stable dispersion and the attachment of this molecule via a
14 Meisenheimer complex increased the graphene's dispersibility in MeCN to give indefinitely
15 stable solutions at concentrations of 0.9 mg mL⁻¹. The UV-Vis absorption spectra of
16 exfoliated graphene, functionalized graphene, and Meisenheimer complex graphene
17 dispersions in MeCN (**Figure 6c**) support the proposed structures. The characteristic feature
18 at 270 nm, corresponds to a π - π^* plasmon peak where van Hove singularities occur.^[39] For
19 the functionalized graphene, this peak blue-shifts to ~195.5 nm, suggesting that the electronic
20 conjugation within the graphene was severely restricted by the sp^3 defects.^[37, 40, 41] After
21 functionalization, a new absorbance peak associated with the 3,5-DiNP group appeared at
22 249.1 nm (**Figure 6c and Figure S13**). The strongly electron-withdrawing nitro groups in 3,5-
23 dinitrobenzene favor Meisenheimer complexes with primary amines.^[42] This chemical
24 characteristic is preserved in 3,5-DiNP functionalized graphene and **Figure 6a** illustrates the
25 formation of Meisenheimer complex with *n*-butylamine. The Meisenheimer complex
26 graphene produces only small variations in the optical spectra (**Figure 6c**), however, the
27 complex is confirmed by a weakening of the NO₂ infrared bands with a -7.9 cm^{-1} shift on
28 $\nu_{\text{asym}}(\text{N-O})$ and -1.5 cm^{-1} on $\nu_{\text{sym}}(\text{N-O})$ (**Figure 6d**). The capability of functionalized
29
30
31
32
33
34
35
36
37
38
39
40
41
42
43
44
45
46
47
48
49
50
51
52
53
54
55
56
57
58
59
60
61
62
63
64
65

graphene to form Meisenheimer complex provides a new method to control electronic structure and conjugate to biologically relevant species.

To conclude, we have developed a method for spontaneous exfoliation of highly functionalized graphene directly from Hyper-3-Stage-1 GIC by reaction with an aryl diazonium salt solution under electrochemical reducing conditions. The successful covalent functionalization of the sp^2 carbon network of graphene with one group per 12 graphene C was obtained by first weakening the van der Waals attractions between graphene sheets by cation- π interacted GICs. Key to this process is a reduction of the organization (crystallinity) of the intercalated ions, which is accomplished by partial reductive decomposition of the TBA⁺ cations. Highly expanded graphenes, characterized as Hyper-3-Stage-1 GIC (d_{001} -spacing > 15.3 Å) were produced without any evidence of creating new covalent defects that disrupt the sp^2 lattice. The different intermediate Hyper-Stage-1 GICs were unambiguously characterized by XRD, Raman spectroscopy, TEM and XPS. Raman analysis further confirmed the conversion of delocalized graphene sp^2 states to localized sp^3 bonds with the functionalization with 3,5-DiNP groups. The formation of a Meisenheimer complex between 3,5-dinitrobenzene functionalized graphene with amines has utility for creating new forms of functional graphenes.

Supporting Information

Supporting Information is available from the Wiley Online Library or from the author.

Acknowledgements

This work was financially supported by the National Science Foundation, DMR-1410718.

Received: ((will be filled in by the editorial staff))

Revised: ((will be filled in by the editorial staff))

Published online: ((will be filled in by the editorial staff))

References

- [1] A. K. Geim, K. S. Novoselov, *Nat. Mater.* **2007**, *6*, 183.

- [2] C. Lee, X. D. Wei, J. W. Kysar, J. Hone, *Science* **2008**, *321*, 385.
- [3] A. A. Balandin, *Nat. Mater.* **2011**, *10*, 569.
- [4] K. S. Novoselov, V. I. Fal'ko, L. Colombo, P. R. Gellert, M. G. Schwab, K. Kim, *Nature* **2012**, *490*, 192.
- [5] T. M. Swager, *ACS Macro. Lett.* **2012**, *1*, 3.
- [6] V. Georgakilas, M. Otyepka, A. B. Bourlinos, V. Chandra, N. Kim, K. C. Kemp, P. Hobza, R. Zboril, K. S. Kim, *Chem. Rev.* **2012**, *112*, 6156.
- [7] D. R. Dreyer, S. Park, C. W. Bielawski, R. S. Ruoff, *Chem. Soc. Rev.* **2010**, *39*, 228.
- [8] C. K. Chua, M. Pumera, *Chem. Soc. Rev.* **2014**, *43*, 291.
- [9] C. J. Shih, A. Vijayaraghavan, R. Krishnan, R. Sharma, J. H. Han, M. H. Ham, Z. Jin, S. C. Lin, G. L. C. Paulus, N. F. Reuel, Q. H. Wang, D. Blankschtein, M. S. Strano, *Nat. Nanotechnol.* **2011**, *6*, 439.
- [10] N. I. Kovtyukhova, Y. X. Wang, A. Berkdemir, R. Cruz-Silva, M. Terrones, V. H. Crespi, T. E. Mallouk, *Nat. Chem.* **2014**, *6*, 957.
- [11] M. S. Dresselhaus, G. Dresselhaus, *Adv. Phys.* **1981**, *30*, 139.
- [12] A. M. Dimiev, G. Ceriotti, N. Behabtu, D. Zakhidov, M. Pasquali, R. Saito, J. M. Tour, *ACS Nano* **2013**, *7*, 2773.
- [13] G. L. Doll, P. C. Eklund, J. E. Fischer, *Phys. Rev. B* **1987**, *36*, 4940.
- [14] G. L. C. Paulus, Q. H. Wang, M. S. Strano, *Acc. Chem. Res.* **2013**, *46*, 160.
- [15] M. Lotya, Y. Hernandez, P. J. King, R. J. Smith, V. Nicolosi, L. S. Karlsson, F. M. Blighe, S. De, Z. M. Wang, I. T. McGovern, G. S. Duesberg, J. N. Coleman, *J. Am. Chem. Soc.* **2009**, *131*, 3611.
- [16] Y. L. Zhong, T. M. Swager, *J. Am. Chem. Soc.* **2012**, *134*, 17896.
- [17] A. S. Mahadevi, G. N. Sastry, *Chem. Rev.* **2013**, *113*, 2100.
- [18] J. C. Chacon-Torres, L. Wirtz, T. Pichler, *Phys. Status Solidi B* **2014**, *251*, 2337.
- [19] W. Sirisaksoontorn, A. A. Adenuga, V. T. Remcho, M. M. Lerner, *J. Am. Chem. Soc.* **2011**, *133*, 12436.
- [20] A. J. Fry, R. L. Krieger, *J. Org. Chem.* **1976**, *41*, 54.
- [21] A. C. Ferrari, *Solid State Commun.* **2007**, *143*, 47.
- [22] J. K. Liu, Q. Q. Li, Y. Zou, Q. K. Qian, Y. H. Jin, G. H. Li, K. L. Jiang, S. S. Fan, *Nano Lett* **2013**, *13*, 6170.
- [23] R. J. Nemanich, S. A. Solin, D. Guerard, *Phys. Rev. B* **1977**, *16*, 2665.
- [24] A. Das, S. Pisana, B. Chakraborty, S. Piscanec, S. K. Saha, U. V. Waghmare, K. S. Novoselov, H. R. Krishnamurthy, A. K. Geim, A. C. Ferrari, A. K. Sood, *Nat. Nanotechnol.* **2008**, *3*, 210.
- [25] P. T. Araujo, D. L. Mafra, K. Sato, R. Saito, J. Kong, M. S. Dresselhaus, *Phys. Rev. Lett.* **2012**, *109*, 046801.
- [26] J. U. Lee, D. Yoon, H. Cheong, *Nano Lett.* **2012**, *12*, 4444.
- [27] O. Frank, M. Mohr, J. Maultzsch, C. Thomsen, I. Riaz, R. Jalil, K. S. Novoselov, G. Tsoukleri, J. Parthenios, K. Papagelis, L. Kavan, C. Galiotis, *ACS Nano* **2011**, *5*, 2231.
- [28] O. Frank, G. Tsoukleri, J. Parthenios, K. Papagelis, I. Riaz, R. Jalil, K. S. Novoselov, C. Galiotis, *ACS Nano* **2010**, *4*, 3131.
- [29] M. J. Webb, P. Palmgren, P. Pal, O. Karis, H. Grennberg, *Carbon* **2011**, *49*, 3242.
- [30] G. Muilenberg, *Perkin-Elmer Corporation* **1979**.
- [31] L. C. Ma, L. H. Meng, Y. W. Wang, G. S. Wu, D. P. Fan, J. L. Yu, M. W. Qi, Y. D. Huang, *RSC Adv.* **2014**, *4*, 39156.
- [32] F. Volatron, J. M. Noel, C. Rinfray, P. Decorse, C. Combellas, F. Kanoufi, A. Proust, *J. Mater. Chem. C* **2015**, *3*, 6266.
- [33] E. Bekyarova, M. E. Itkis, P. Ramesh, C. Berger, M. Sprinkle, W. A. de Heer, R. C. Haddon, *J. Am. Chem. Soc.* **2009**, *131*, 1336.

- 1 [34] Q. Z. Wu, Y. P. Wu, Y. F. Hao, J. X. Geng, M. Charlton, S. S. Chen, Y. J. Ren, H. X.
2 Ji, H. F. Li, D. W. Boukhvalov, R. D. Piner, C. W. Bielawski, R. S. Ruoff, *Chem. Commun.*
3 **2013**, 49, 677.
- 4 [35] W. Richard, D. Evrard, P. Gros, *J. Electroanal. Chem.* **2012**, 685, 109.
- 5 [36] A. Dato, V. Radmilovic, Z. Lee, J. Phillips, M. Frenklach, *Nano Lett.* **2008**, 8, 2012.
- 6 [37] J. M. Englert, C. Dotzer, G. A. Yang, M. Schmid, C. Papp, J. M. Gottfried, H. P.
7 Steinruck, E. Spiecker, F. Hauke, A. Hirsch, *Nat. Chem.* **2011**, 3, 279.
- 8 [38] D. A. C. Brownson, D. K. Kampouris, C. E. Banks, *Chem. Soc. Rev.* **2012**, 41, 6944.
- 9 [39] D. Li, M. B. Muller, S. Gilje, R. B. Kaner, G. G. Wallace, *Nat. Nanotechnol.* **2008**, 3,
10 101.
- 11 [40] G. Eda, Y. Y. Lin, C. Mattevi, H. Yamaguchi, H. A. Chen, I. S. Chen, C. W. Chen, M.
12 Chhowalla, *Adv. Mater.* **2010**, 22, 505.
- 13 [41] J. Robertson, E. P. O'Reilly, *Phy. Rev. B, Condens. Matter* **1987**, 35, 2946.
- 14 [42] G. A. Artamkina, M. P. Egorov, I. P. Beletskaya, *Chem. Rev.* **1982**, 82, 427.
- 15
16
17
18
19
20
21
22
23
24
25
26
27
28
29
30
31
32
33
34
35
36
37
38
39
40
41
42
43
44
45
46
47
48
49
50
51
52
53
54
55
56
57
58
59
60
61
62
63
64
65

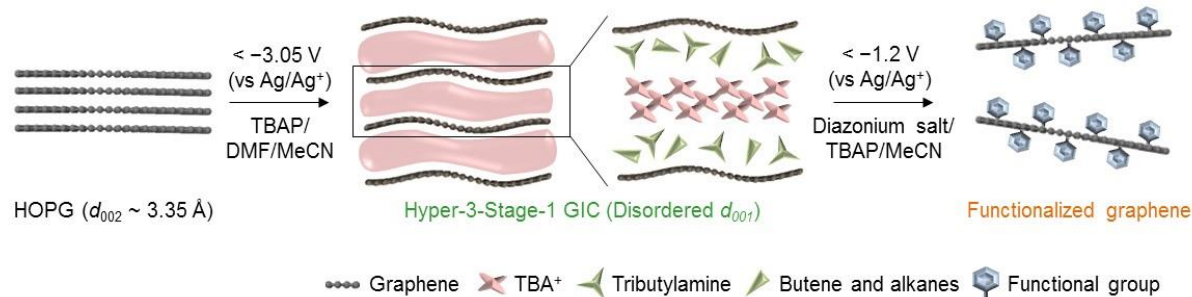


Figure 1. Illustration of the generation of a Hyperstage-1-GIC by electrochemical intercalation of TBA⁺ ions and amine generation. This periodic solid reacts with diazonium ions and spontaneously exfoliates (disperses) to form solutions of functionalized graphenes.

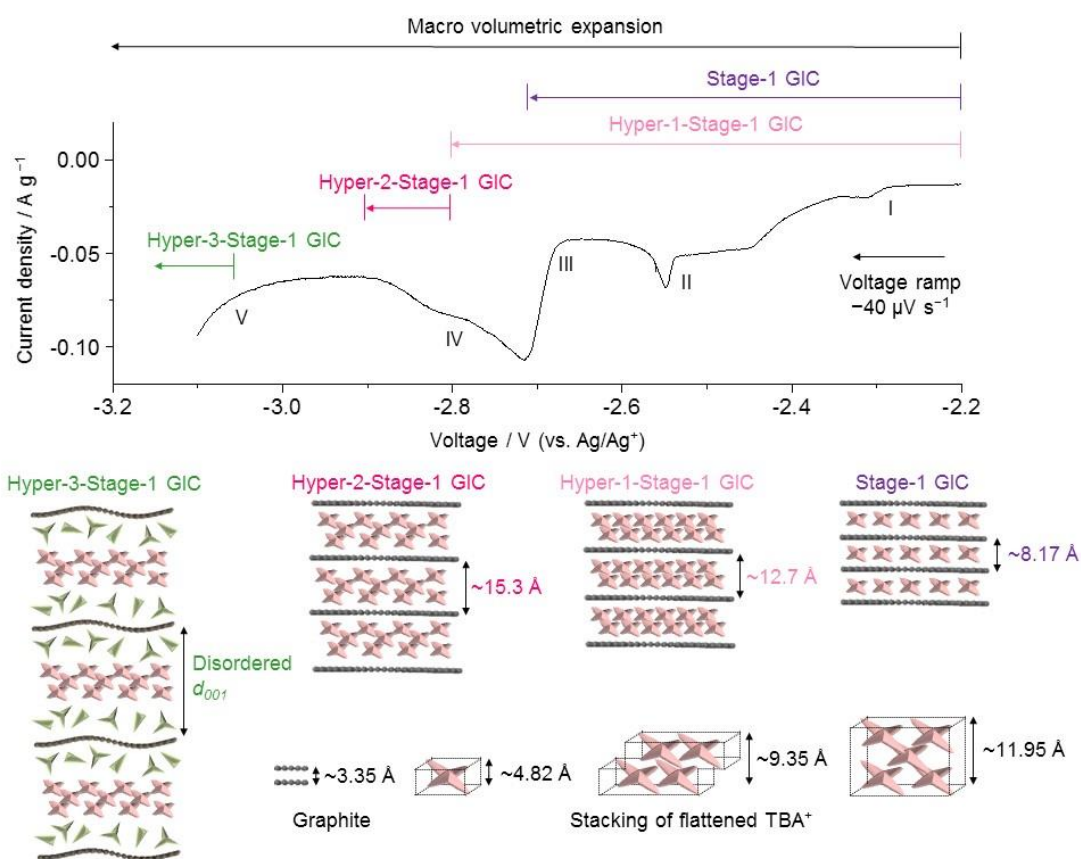


Figure 2. Voltage sweep of HOPG working electrode with a graphite counter electrode and Ag/Ag⁺ reference electrode, in 1.5 M tetrabutylammonium perchlorate (TBAP) in MeCN/DMF, recorded at scan rates of $-40 \mu\text{V s}^{-1}$ at 25 °C. The structural models of the associated GICs illustrate the different levels of intercalation and interlayer spacing. Linear

voltage ramping conditions: Stage-1 ($-40 \mu\text{V s}^{-1}$), Hyper-1-Stage-1 ($-40 \mu\text{V s}^{-1}$), Hyper-2-Stage-1 ($-2 \mu\text{V s}^{-1}$) and Hyper-3-Stage-1 GIC ($-3 \mu\text{V s}^{-1}$).

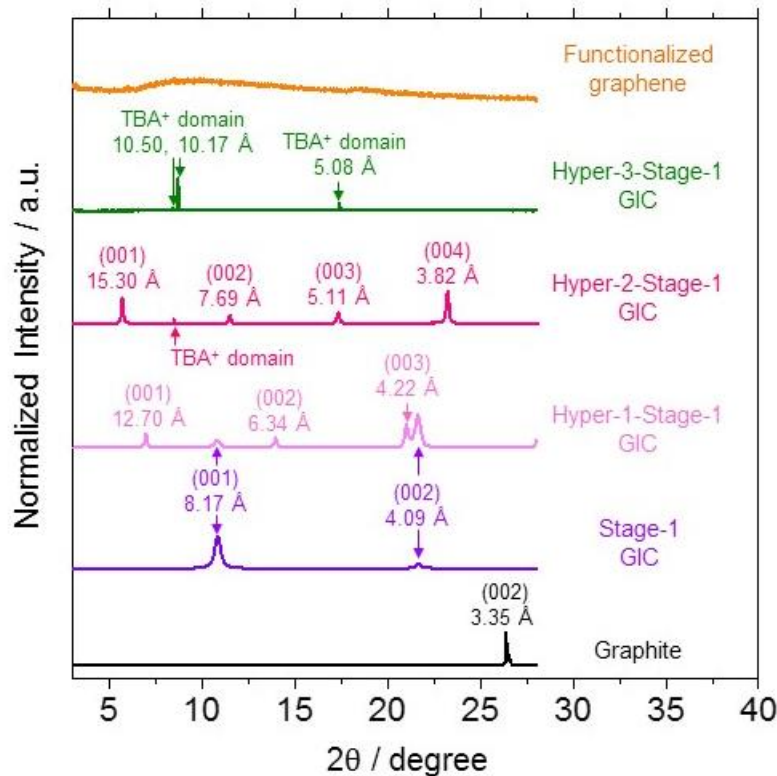


Figure 3. XRD diffraction data of HOPG at different levels of electrochemical activation. Stage-1, Hyper-1-Stage-1, Hyper-2-Stage-1 and Hyper-3-Stage-1 GICs and functionalized graphene. The additional peaks, not related to graphene stacking, appeared at around 8.4 and 8.7° are assigned to the organized TBA⁺ domains in Hyper-2-Stage-1 and Hyper-3-Stage-1 GICs.

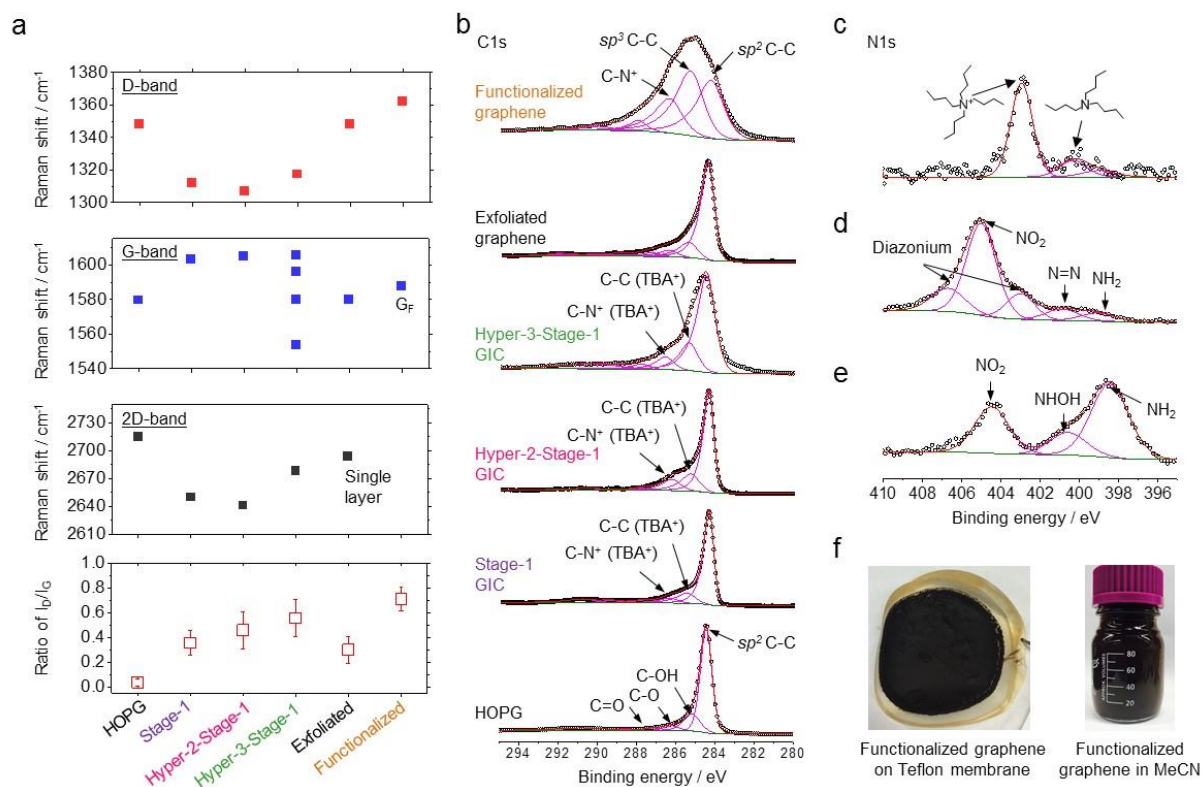


Figure 4. Comparison of the Raman and XPS spectra of HOPG, GICs, exfoliated graphene and functionalized graphene. (a) Measured *ex-situ* Raman data points (D, G and 2D-bands) of HOPG, Stage-1, Hyper-2-Stage-1 GIC, Hyper-3-Stage-1 GICs, exfoliated graphene and functionalized graphene. (b) High resolution XPS spectra (black circles) of HOPG, Stage-1, Hyper-2-Stage-1, Hyper-3-Stage-1 GICs, exfoliated graphene, and functionalized graphene (Magenta: Lorentzian/Gaussian peak fitting, red: convoluted line and green: Shirley based line) in the region of C 1s. High resolution N 1s spectra of (c) Hyper-3-Stage-1 GIC (d) 3,5-dinitrobenzenediazonium as a reference and (e) functionalized graphene with 3,5-dinitrophenyl 3,5-DiNP groups. (f) Photographs showing functionalized graphene with 3,5-DiNP groups on a polytetrafluoroethylene (PTFE) filter membrane (left) and in MeCN (right).

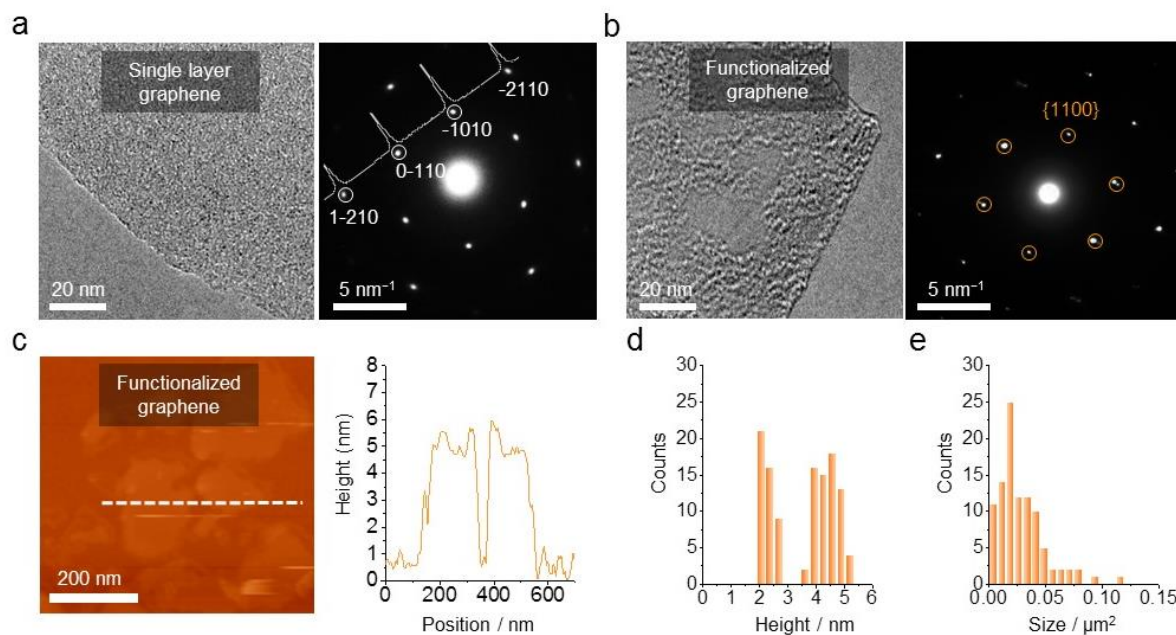


Figure 5. TEM and AFM characterization of graphenes. (a) TEM micrograph and electron diffraction patterns of a graphene produced by ultrasonic assisted dispersion of Hyper-3-stage 1 GIC. The crystal lattice retains its characteristic hexagonal diffraction peaks (1–210), (0–110), (–1010), and (–2110) diffractions. (b) TEM of functionalized graphene produced from diazonium ion reactions with Hyper-3-stage 1 GIC. This material shows apparent domains of functionalization but it still maintains a {1100} diffraction pattern. (c) **Topographic image on mica by AFM of functionalized graphene and a height profile measured along the white dashed line.** The height distribution and particle size of the functionalized graphenes are shown in (d) and (e), respectively.

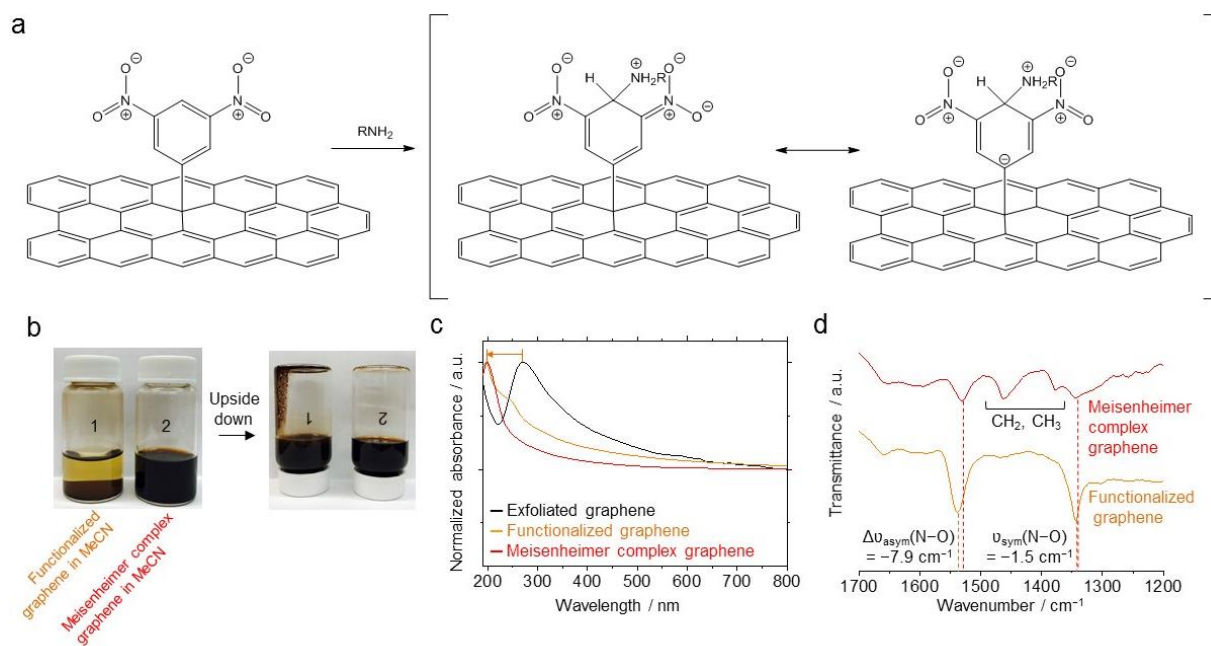


Figure 6. Meisenheimer complex graphenes produced by reactions with amines. (a) Proposed mechanism for the formation of Meisenheimer complex graphene, wherein pendant 3,5-DiNP groups react with *n*-butylamine ($\text{R} = n\text{-butyl}$) (b) The photographs of MeCN solutions of functionalized graphene with 3,5-DiNP groups and the Meisenheimer complex graphene (dispersions after 1 day). (c) Normalized absorption spectrum of exfoliated graphene, graphene with 3,5-DiNP groups, and the *n*-butylamine Meisenheimer complex graphene in MeCN. The $\pi \rightarrow \pi^*$ plasmon peak of the graphene is blue shifted (yellow arrow: -74.5 nm) after the functionalization. (d) ATR-FTIR spectra of functionalized graphene with 3,5-DiNP groups and formation of the Meisenheimer complex graphene results in changes in the NO₂ bands.

Hyperstage-1 graphite intercalation compound (GIC) has a very large interlayer spacing $d_{001} > 15.3 \text{ \AA}$ and contains disordered interstitial molecules/ions. The GIC is highly activated and undergoes spontaneous exfoliation when reacted with diazonium ions to produce soluble graphenes with high functionalization densities of one pendant aromatic ring for every 12 graphene carbons.

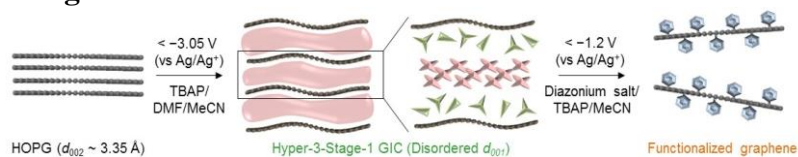
Keyword

Hyperstage-1 graphite intercalation compound, spontaneous exfoliation, functionalized graphene, diazonium salt, Meisenheimer complex

Intak Jeon, Bora Yoon, Maggie He, and Timothy M. Swager*

Hyperstage Graphite: Electrochemical Synthesis and Spontaneous Reactive Exfoliation

ToC figure



Supporting Information

Hyperstage Graphite: Electrochemical Synthesis and Spontaneous Reactive Exfoliation

*Intak Jeon, Bora Yoon, Maggie He, and Timothy M. Swager**

I. Jeon

Department of Materials Science and Engineering, Institute for Soldier Nanotechnologies
Massachusetts Institute of Technology
Cambridge, Massachusetts 02139, USA

B. Yoon, M. He, and T. M. Swager

Department of Chemistry, Institute for Soldier Nanotechnologies
Massachusetts Institute of Technology
Cambridge, Massachusetts 02139, USA
E-mail: tswager@mit.edu

Experimental Section

Electrochemical intercalation of graphite: HOPG intercalation was carried out in anhydrous DMF (2 mL) and MeCN (2 mL, dried over 3 Å molecular sieves) containing 1.5 M TBAP under N₂ atmosphere. HOPG was connected to both negative and positive terminals of a potentiostat via alligator clips. The reference electrode was non-aqueous Ag/Ag⁺. (Note: at high negative voltage (~ -1.3 V), electrolysis of water disrupts the electrical contact of graphite domains and prevents effective intercalation, dry solvents are necessary for effective *in-situ* intercalation). Linear voltage ramping conditions: -2.2 to -2.7 V at -40 μV s⁻¹ for Stage-1 GIC, -2.2 to -2.8 V at -40 μV s⁻¹ for Hyper-1-Stage-1 GIC, -2.8 to -2.9 V at -2 μV s⁻¹ for Hyper-2-Stage-1 GIC and -3.05 to -3.15 V at -3 μV s⁻¹ for Hyper-3-Stage-1 GIC. Applying a negative bias voltage results in intercalations of TBA⁺ cations, starting at the edges of graphite. When a voltage was applied, the morphology of graphite edges changed drastically within a few seconds. The edge of the graphite continued to expand and the increase in the thickness of the graphite layers can be observed visually.

1
2
3
4
5
6
7
8
9
10
11
12
13
14
15
16
17
18
19
20
21
22
23
24
25
26
27
28
29
30
31
32
33
34
35
36
37
38
39
40
41
42
43
44
45
46
47
48
49
50
51
52
53
54
55
56
57
58
59
60
61
62
63
64
65

Synthesis of 3,5-dinitrobenzenediazonium tetrafluoroborate:^[1] 3,5-dinitroaniline (1.83 g, 10.0 mmol) was dissolved in a mixture of tetrafluoroboric acid (48 wt%, 3.4 mL) and Milli-Q H₂O (1.5 mL). The mixture was cooled to 0°C. A solution of sodium nitrite (690 mg, 10.0 mmol) in Milli-Q H₂O (4.0 mL) was added slowly from behind a shield. (Note: diazonium salts are potentially explosive, a blast shield was used throughout the reaction.) The reaction was stirred vigorously for 30 min at 0 °C and filtered through a Büchner funnel. The solid was dissolved in minimum amount of acetone and the product was precipitated by addition of cold Et₂O. Pure 3,5-dinitrobenzenediazonium tetrafluoroborate (2.09 g, 74%) was collected by filtration through a Büchner funnel. ¹H NMR (400 MHz, Acetonitrile-*d*₃) δ 9.58 (d, *J* = 2.0 Hz, 2H), 9.50 (t, *J* = 2.0 Hz, 1H). ¹⁹F NMR (376 MHz, Acetonitrile-*d*₃) δ -151.10, -151.16. ¹³C NMR (126 MHz, Acetonitrile-*d*₃) δ 150.10, 133.53, 131.60, 119.66. ESI-HRMS: calculated for C₆H₃N₄O₃⁺ [M]⁺: 195.0149, found: 195.0158.

31
32
33
34
35
36
37
38
39
40
41
42
43
44
45
46
47
48
49
50
51
52
53
54
55
56
57
58
59
60
61
62
63
64
65

Electrochemical functionalization of graphene with 3,5-dinitrobenzenediazonium salt: In-situ functionalization was carried out by immersing Hyper-3-Stage-1 GIC in MeCN (4 mL) containing 0.1 M 3,5-dinitrobenzenediazonium tetrafluoroborate and 1 M TBAP under N₂ atmosphere. The voltage was linearly increased from -1.2 V to -2.2 V (vs Ag/AgNO₃). During electrochemical grafting, nitrogen bubbles evolving from Hyper-3-Stage-1 GIC were observed. The functionalized graphene was then dispersed in MeCN by ultrasonication for a short time (e.g. 10 secs). Extensive washing steps were carried out to remove unreacted reagents and byproducts. Functionalized graphene was collected through a PTFE filter membrane with 0.1 μm pore size by vacuum filtration. A dispersion was used for characterization. We did not use supernatant/centrifuged functionalized graphene dispersion. The resultant functionalized graphenes are isolated from acetonitrile solutions and the purified materials were obtained by simple filtration followed by washing with solvents. The more ordered Hyper-1-Stage-1 GIC and Hyper-2-Stage-1 GIC have entirely crystalline TBA⁺

intercalation layers do not spontaneous exfoliation in spite of large graphene intersheet spacing when exposed to solutions containing reactive diazonium ions these material.

Mechanical exfoliation and analysis at the various levels of electrochemical activation, in the absence of diazonium ions, generates pristine defect free unfunctionalized graphenes. Samples were prepared by simple spin- or drop-casting of the functionalized graphene dispersion in MeCN onto substrates for Raman, IR, AFM, XPS and TEM. Exfoliated unfunctionalized graphene dispersion was prepared by ultrasonicing Hyper-3-Stage-1 in DMF overnight. The dispersion was filtered through a 0.1 μm pore Teflon membrane.

HOPG electrochemical intercalation

As shown in **Figure 1 in the main text**, scanning from -2.2 to -3.1 V resulted in clear cathodic peaks currents associated with the intercalation of TBA^+ into the graphene galleries. The low intensity and broaden breadth of (00ℓ) reflections indicated less degree of ordering along the c axis, compared with those of highly oriented pyrolytic graphite (HOPG). The graphite staging phenomenon is related to the periodic sequence of graphene gallery and intercalant layers, which is distinct from disintegration of graphite domains. Graphite intercalation compounds (GICs) are defined as compositions wherein atomic or molecular layers of the intercalant are inserted between the layers of graphite host material. GICs are classified in stages 1, 2, ..., n , where stage n means that one intercalant layer follows after n graphene layers.^[2] The stage index n is given by the relation $L_c = (n - 1)C_o + d_s$ where C_o is the distance between adjacent graphite layers ($C_o = 3.35 \text{ \AA}$) and d_s is the distance between two graphene layers with an intercalant layer in between. The crystallographic evidence confirmed that tetrabutylammonium (TBA^+) cations intercalated every graphene layers. The applied negative potential resulted in diffusion of TBA^+ cations into the graphene galleries, forming TBA^+ -GIC. When the initial potential was above around -2.80 V (Ag/Ag^+), a Hyper-2-Stage-1 GIC was fully obtainable. As-prepared Stage-1 GIC was not able to be fully

converted to Hyper-2-Stage-1 GIC even the final voltage was applied above -3.15 V. Depending on the potentials, the d_{001} spacing of GIC evolved from 8.17 to 12.7 to 15.3 Å in **Figure S1**. The Hyper-1-Stage-1 and Hyper-2-Stage-1 contained more intercalated TBA^+ than Stage-1 GIC, maintaining every graphene sheet separated. They were not Stage- n ($n = 2, 3$ and 4). In addition, graphene grain boundaries (nanoscale width) on a HOPG are not visible using optical microscope.^[3] We can determine whether the intercalation process occurs or not through colors/contrasts of GICs using the optical image as shown in **Figure S1**. After TBA^+ -intercalation the domain boundaries of GICs were clearly distinguishable on the basis of contrast levels. It is interesting to note the surface contrast of GIC was similar as the few layer graphenes, indicating a single/few layer graphene sheets were separated or isolated.^[4] Hyper-3-Stage-1 GIC was achieved through voltage ramp from -3.05 V to -3.15 V (vs Ag/Ag^+) with an associated physical d -spacing expansion of graphite. The expected values (8.15 , 12.95 and 15.35 Å) of d_{001} -spacing of Stage-1, Hyper-1-Stage-1 and Hyper-2-Stage-1 with the height of flattened TBA^+ layer (~ 4.8 Å) and graphene (3.35 Å) matched with x-ray diffraction (XRD) data. The initial applied potential plays a crucial role in the generation of each Hyperstage-1 GIC. Full Hyper-1-Stage-1 GIC was not obtained because the reduction potentials for Hyper-1-Stage-1 and Hyper-2-Stage-1 GICs were overlapped.

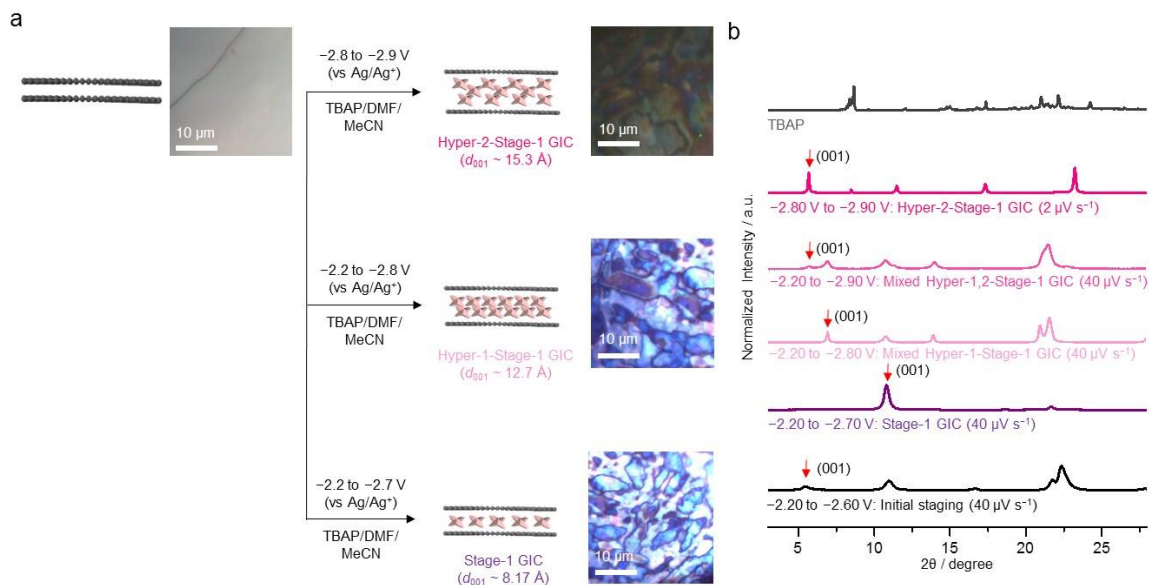


Figure S1. (a) Schematic illustration and electrochemical reaction conditions of the Stage-1, Hyper-1-Stage-1 and Hyper-2-Stage-1 GICs. Optical images of HOPG, Stage-1, Hyper-1-Stage-1 and Hyper-2-Stage-1 GICs. (b) XRD spectra of initial staging, Stage-1, Hyper-1-Stage-1 and Hyper-2-Stage-1 GICs and tetrabutylammonium perchlorate (TBAP).

Interlayer distances for HOPG and different GICs

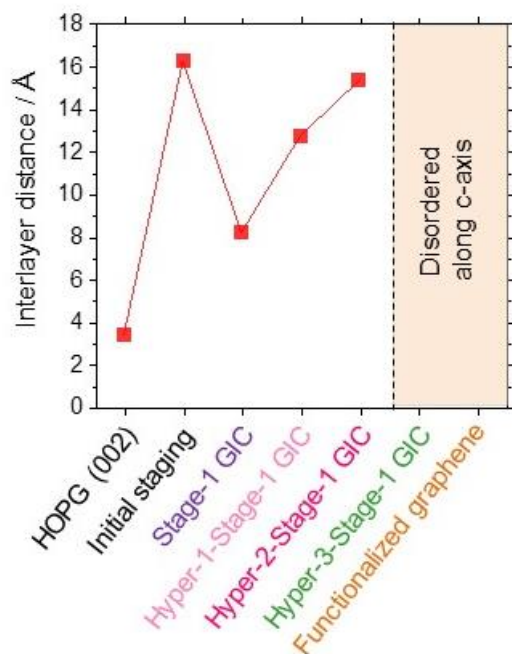


Figure S2. The interlayer distance for HOPG (d_{002}), initial staging (d_{001}), Stage-1 (d_{001}), Hyper-2-Stage-1 (d_{001}), Hyper-3-Stage-1 (*disordered*) GIC and functionalized graphene (*disordered*).

Proposed reduction mechanism of TBA⁺

Our proposed mechanism is that TBA⁺ in the graphene galleries can be decomposed into tributylamine ($n\text{-Bu}_3\text{N}$), butene and alkanes which were trapped in the graphene galleries in **Figure S3a**. The volume of Hyper-3-Stage-1 GIC in the graphene galleries expanded in vacuum **Figure S3b**, indicating that gases are trapped in the graphene galleries. The TBA⁺ acted as a frame to make electrical contacts between graphene galleries. The disordered graphene galleries provided the space where electrochemical electron transfer occurred between the basal plane of graphene and diazonium salt.

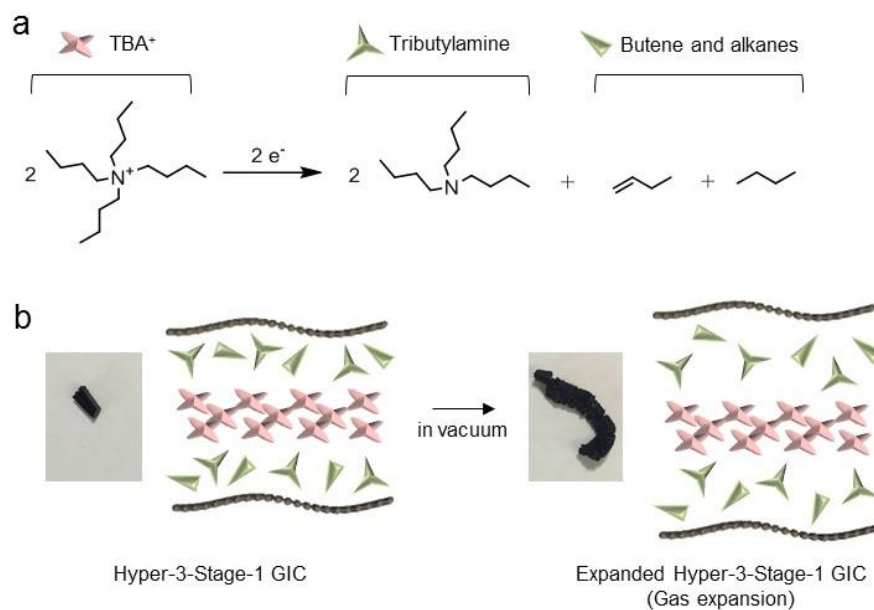


Figure S3. (a) Proposed reduction mechanism of TBA⁺ in Hyper-3-Stage-1 GIC. (b) Photographs of a piece of Hyper-3-Stage-1 and expanded Hyper-3-Stage-1 GIC after drying under reduced pressure at 150°C.

To confirm the electrochemical decomposition of TBA⁺ to *n*-Bu₃N inside the graphene galleries, several NMR measurements were conducted (**Figure S4**). After graphene intercalation was completed, an aliquot of the graphene electrolyte solution was removed and the ¹H NMR was measured (**Figure S4**). No trace of *n*-Bu₃N was observed in this case. This indicated that TBA⁺ decomposition did not occur on the surface of GIC and the decomposed TBA⁺ inside the GIC did not diffuse into the intercalation electrolyte solution. In another experiment, the GIC was transferred to a fresh solution of MeCN (~ 2 mL) and ultrasonication was applied to the mixture in order to exfoliate the GIC and release the intercalated ions and molecules into solution. The ¹H NMR of the resulting GIC dispersion in MeCN was measured and we observed the presence of tributylamine –NCH₂– and –CH₃ protons. This showed that TBA⁺ indeed underwent partial electrochemical decomposition and the decomposed product, tributylamine, was trapped inside the graphene galleries. The six –CH₂– protons of tributylamine overlapped with the –CH₂– protons of TBAP, therefore we

cannot distinguish them. The ^1H NMR of tributylamine and TBAP (**Figure S4**) were overlaid with the above-mentioned spectra for peak identification and comparison.

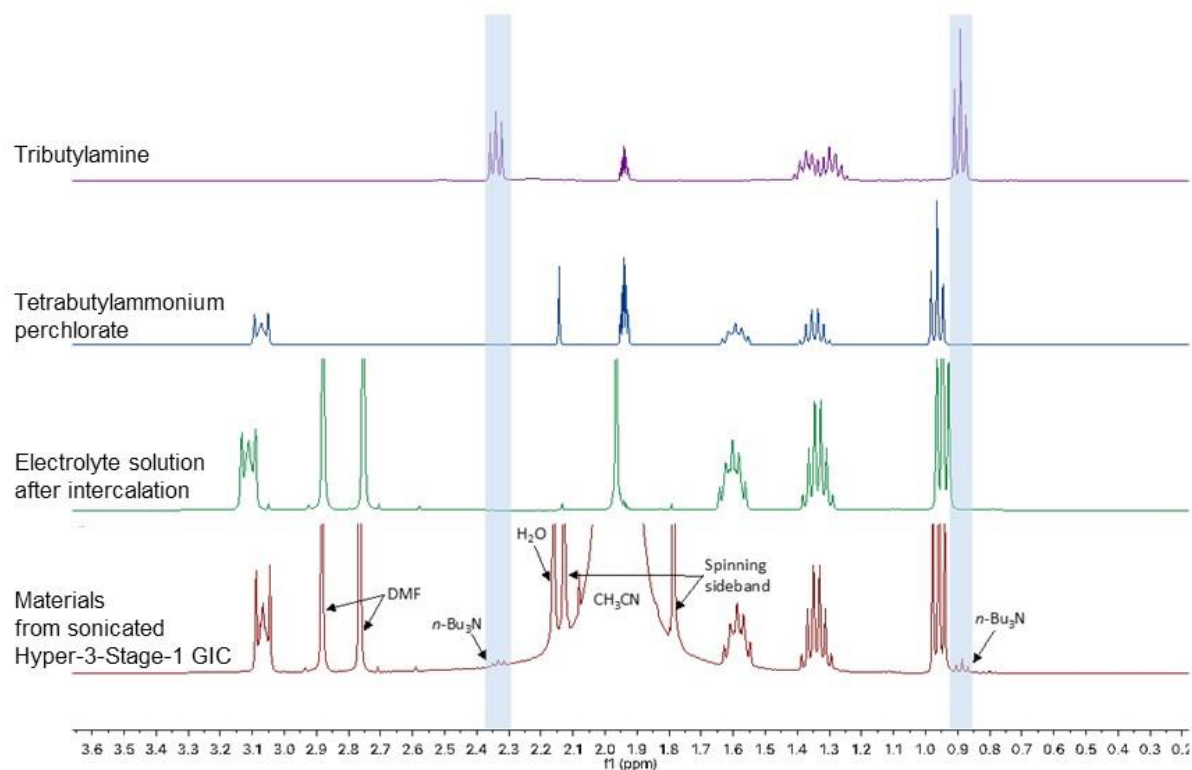


Figure S4. ^1H NMR spectra of tributylamine, TBAP electrolyte solution after intercalation and the GIC dispersion in acetonitrile (MeCN). All ^1H NMR were measured in CD_3CN .

Electrochemical functionalization of Hyper-3-Stage-1 GIC

The functionalization on the basal planes of graphenes in Hyper-3-Stage-1 GIC required higher electrochemical reduction potential than that for graphite surface. This high negative voltage (from -1.2 V) induced migration of solvated TBA^+ /diazonium ions into the graphene interlayers (**Figure S5**). The delocalized π -electrons of the basal plane of graphene undergo electron transfer reactions with the aryl diazonium cation, which becomes an aryl radical after dissociation and production of N_2 . Diazonium cations/radicals surrounded by high density of TBA^+ effectively migrated into graphene interlayer. The aryl radical, which is highly reactive, readily forms a covalent bond with a carbon atom in the graphene lattice changing its hybridization to sp^3 C–C bond. The high density of functional groups increased

graphene solubility in MeCN and electrostatic repulsion force between adjacent graphenes assisted the exfoliation of functionalized graphene.

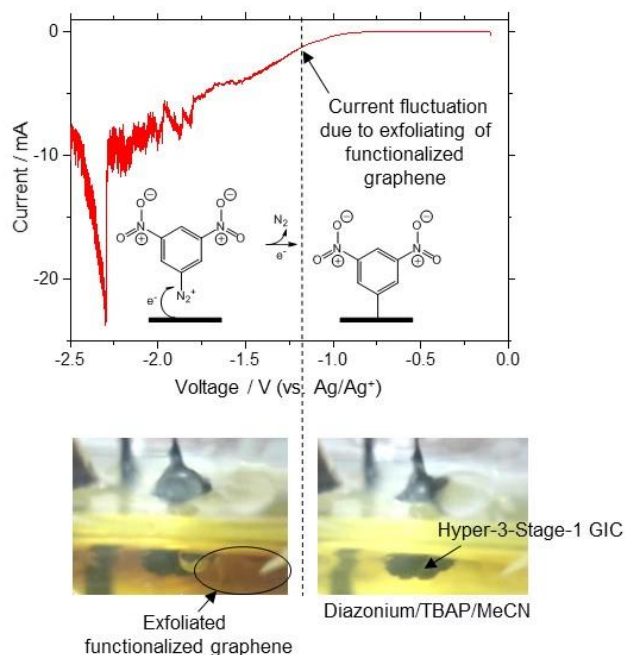


Figure S5. (a) Linear voltage sweep on Hyper-3-Stage-1 GIC (scan rate of $-20 \mu\text{V s}^{-1}$) in 3,5-dinitrobenzenediazonium salt/TBAP/MeCN solution. Proposed electrochemical grafting mechanism on graphene in the presence of diazonium salt. Functionalized graphene is spontaneously exfoliated from Hyper-3-Stage-1 GIC.

Spectroscopic analysis

The basis of the shifts of the G band were observed in the Stage-1 and Hyperstage-1 GICs, indicating all the graphene layers in Stage-1 GICs were individually separated with the nearest graphene. Raman 2D bands of Stage-1 and Hyperstage-1 GICs cannot provide information on individual graphene separation (**Figure S6a and b**). The functionalization induced amorphization/annihilation of the 2D band of graphene (no longer be used to determine the number of layers). XPS spectra (**Figure S6c**) showed large carbon-to-oxygen ratios for Hyperstage-1 GIC ($\text{C/O} \sim 20$) and exfoliated graphene ($\text{C/O} \sim 39$) showed indicating an insignificant degree of oxidation, which was again comparable to that of the

pristine graphite (C/O ~ 54)).^[5, 6] N 1s peaks were observed after extensive washing and filtration of the functionalized graphene with organic solvents and drying the samples in vacuum. No nitrogen was found in the unfunctionalized exfoliated graphene, suggesting that the nitrogen content on the graphene was originated from 3,5-dinitrobenzenediazonium functionalization. The G-band of exfoliated graphene showed a reversible behavior, its frequency and shape returned to that observed for HOPG, after the decoupling of TBA⁺ cations from graphene.

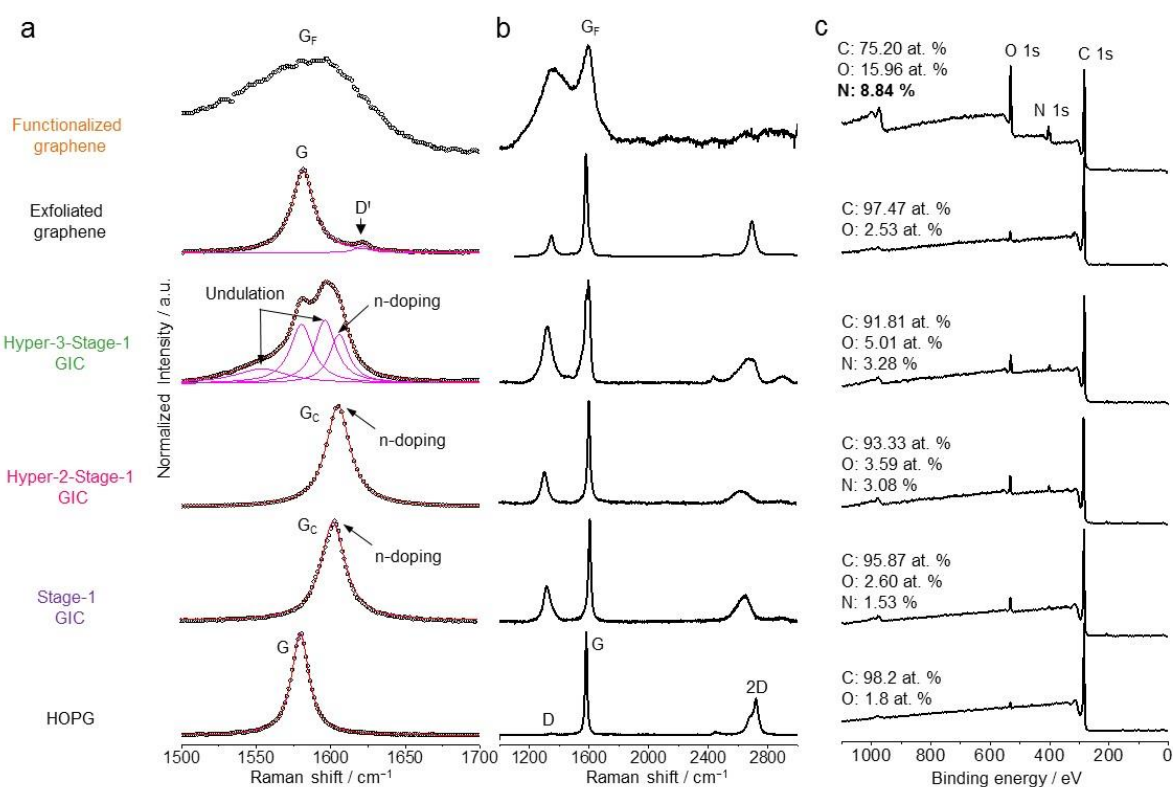
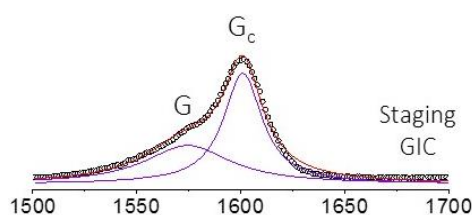


Figure S6. (a) The representative Raman spectra of the G-band of HOPG, Stage-1, Hyper-2-Stage-1, Hyper-3-Stage-1 GICs, exfoliated graphene and functionalized graphene with 3,5-dinitrophenyl (3,5-DiNP) groups. (b) The Raman spectra of HOPG, Stage-1, Hyper-2-Stage-1, Hyper-3-Stage-1 GICs, exfoliated graphene and functionalized graphene with 3,5-DiNP groups. These measurements on samples were taken with a 532 nm excitation laser with SiO₂ (300 nm)/Si substrates. (c) XPS spectra of the survey scans of HOPG, Stage-1, Hyper-2-

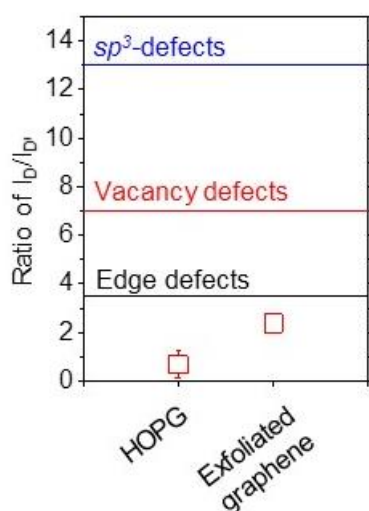
1 Stage-1, Hyper-3-Stage-1 GICs, exfoliated graphene and functionalized graphene with 3,5-
 2 DiNP groups with the information of their atomic percents.
 3
 4
 5
 6

7 The G-band of an initial staging GIC with TBA⁺ split into two Raman peaks. The peak
 8 at lower wave number (G) was resulted from a vibrational mode of the inner graphene layers
 9 adjacent to other graphene layers, while the peak at higher wave number (G_c) was due to a
 10 vibrational mode of the boundary graphene layers adjacent to intercalant layers.
 11
 12
 13
 14
 15
 16
 17



18
 19
 20
 21
 22
 23
 24
 25
 26 **Figure S7.** Raman G band of GIC at an initial staging before forming Stage-1 GIC. G band
 27 split into G and G_c.
 28
 29
 30
 31
 32
 33

34 The Raman I_D/I_{D'} band intensity ratios of HOPG and exfoliated graphene were 0.67
 35 and 2.4, respectively. The D-band of exfoliated graphene was accounted mainly by edge
 36 defects.
 37
 38
 39
 40
 41
 42
 43
 44
 45
 46
 47
 48
 49
 50
 51
 52
 53
 54
 55
 56
 57
 58



59 **Figure S8.** Raman I_D/I_{D'} band intensity ratios of HOPG and exfoliated graphene.
 60
 61
 62
 63
 64
 65

XRD of exfoliated graphene

Dropcasted exfoliated graphene on a substrate displayed a weakly reconstructed diffraction peak at $2\theta = 26.27^\circ$, which is the characteristic (002) reflection of graphite which originated from the interlayer distance between sheets.

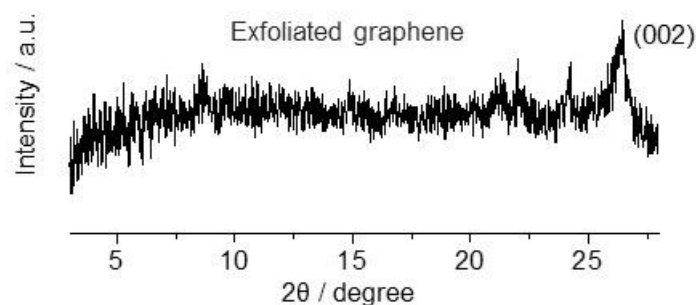


Figure S9. XRD data of exfoliated graphene powder on a zero diffraction substrate after overnight sonication of Hyper-3-Stage-1 GIC in *N,N*-dimethylformamide (DMF).

XPS of Hyper-2-Stage1 and Hyper-3-Stage-1 GICs in diazonium functionalization

Upon application of a higher negative voltage (-3.05 V vs Ag/Ag^+), the intercalated TBA^+ within the graphite sheets decomposed electrochemically (**Figure S10a**). The N 1s XPS spectrum clearly shows the reduced form of TBA^+ in Hyper-3-stage-1 GICs (**Figure S10b**). The area ratio among NO_2 , NHOH and NH_2 on functionalized graphenes with 3,5-DiNP groups shows this dependence on the applied voltages (**Figure S10b**).

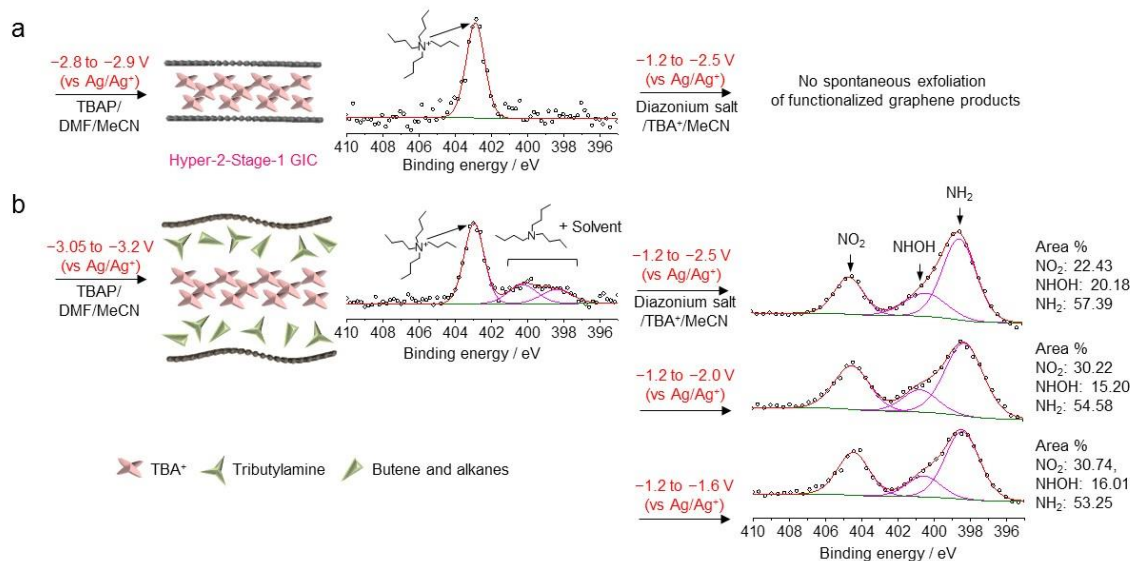


Figure S10. Schematic illustration of the intercalated/decomposed TBA⁺s in Hyper-2-Stage-1 and Hyper-3-Stage-1 GICs. High resolution N 1s spectra of (a) Hyper-2-Stage-1, (b) Hyper-3-Stage-1 GICs and their derivative functionalized graphenes with 3,5-DiNP groups.

ATR-FTIR of 3,5-DiNP functionalized graphene

The peaks located at 1538.9 and 1344.4 cm⁻¹ were attributed to $\nu_{\text{asym}}(\text{N-O})$ and $\nu_{\text{sym}}(\text{N-O})$ bands, respectively.^[8, 9]

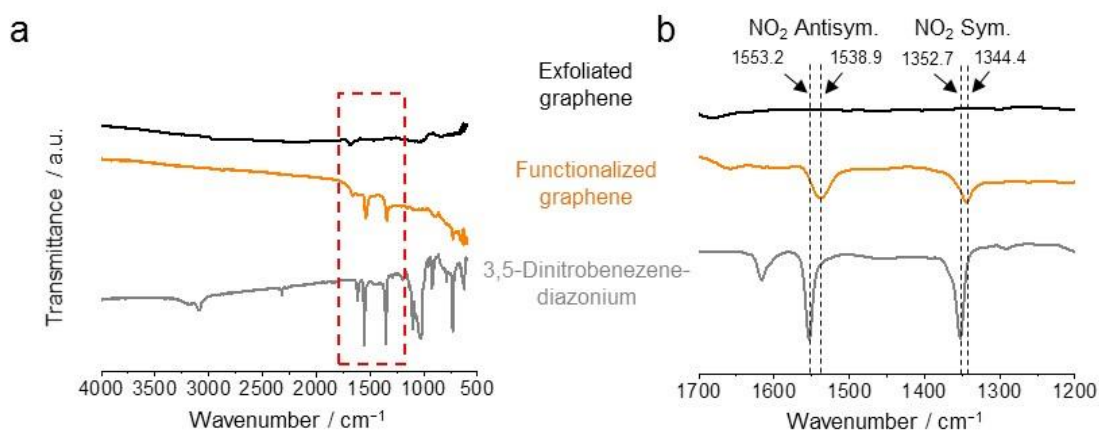


Figure S11. (a) Attenuated total reflection (ATR)-Fourier transform infrared (FTIR) spectrum of exfoliated graphene, functionalized graphene with 3,5-DiNP groups and 3,5-dinitrobenzenediazonium salt. (b) Specific ranges for the nitro stretches.

AFM of 3,5-DiNP functionalized graphene

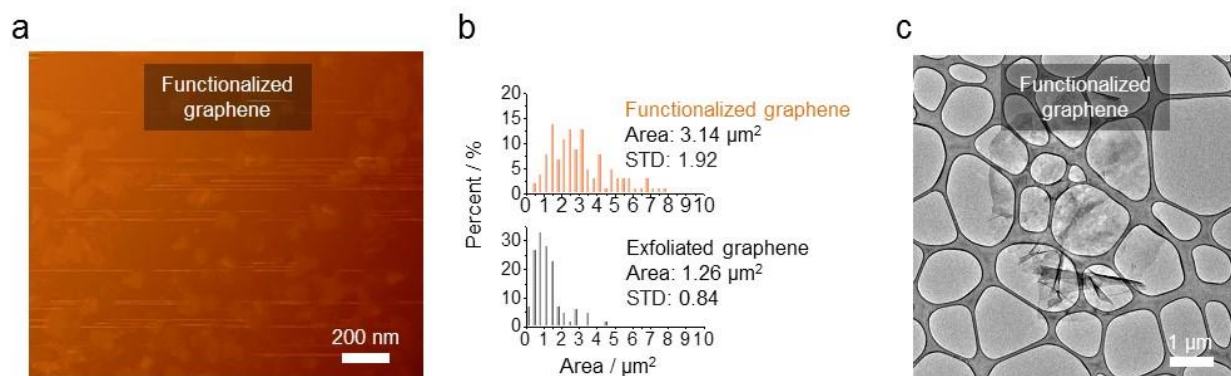


Figure S12. (a) Atomic-force microscopy (AFM) topographic image showing the homogeneously functionalized graphenes with 3,5-DiNP groups on a mica substrate. The functionalized graphene was imaged by AFM by spin coating a dilute (concentration of 0.1 mg mL⁻¹) dispersion on a mica substrate. (b) Area distributions of exfoliated graphene and functionalized graphene with 3,5-DiNP groups obtained by transmission electron microscopy (TEM). (c) TEM micrograph of a representative functionalized graphene with 3,5-DiNP groups deposited over a TEM grid.

We find that the domain size analysis is dependent on the sample preparation and TEM analysis of the dropcast functionalized graphene revealed an average area of $\sim 3.14 \mu\text{m}^2$ (**Figure S12**). The smaller sizes observed in the AFM are likely the result of larger graphenes being removed by centrifugal force experienced with spincoating. The sizes of functionalized graphenes (without centrifugation and decantation) analyzed by TEM and AFM analysis ranged in size from 0.003 to $7.8 \mu\text{m}^2$ and correlate well to the domain size distribution of the starting graphite.^[10]

UV-Vis and ATR-FTIR analysis of Meisenheimer complex

As a control experiment, the absorbance peak of 3,5-dinitrobenzenediazonium with *n*-butylamine shifted from 224 to 236 nm in **Figure S13a**. The peaks for nitro groups on 3,5-

dinitrobenzenediazonium located at 1552.9 and 1351.7 cm^{-1} shifted to 1541.1 and 1347.9 cm^{-1} , respectively in **Figure S13b**.

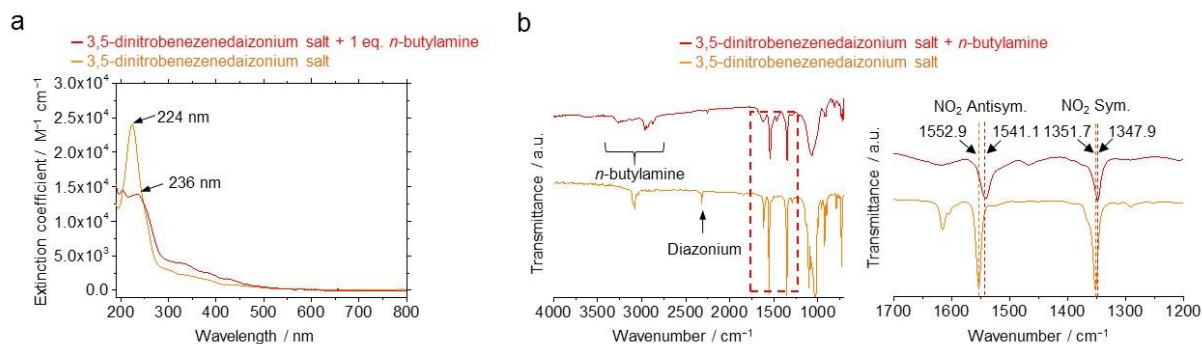


Figure S13. (a) UV-Vis spectra of 3,5-dinitrobenzenediazonium and 3,5-dinitrobenzenediazonium with *n*-butylamine. (b) ATR-FTIR spectra of 3,5-dinitrobenzenediazonium and 3,5-dinitrobenzenediazonium with *n*-butylamine. The changes in NO₂ stretches.

Reference

- [1] P. Hanson, J. R. Jones, A. B. Taylor, P. H. Walton, A. W. Timms, *J. Chem. Soc. Perkin Trans. 2* **2002**, 0, 1135.
- [2] M. S. Dresselhaus, G. Dresselhaus, *Adv. Phys.* **1981**, 30, 139.
- [3] D. L. Duong, G. H. Han, S. M. Lee, F. Gunes, E. S. Kim, S. T. Kim, H. Kim, Q. H. Ta, K. P. So, S. J. Yoon, S. J. Chae, Y. W. Jo, M. H. Park, S. H. Chae, S. C. Lim, J. Y. Choi, Y. H. Lee, *Nature* **2012**, 490, 235.
- [4] Z. H. Ni, H. M. Wang, J. Kasim, H. M. Fan, T. Yu, Y. H. Wu, Y. P. Feng, Z. X. Shen, *Nano Lett.* **2007**, 7, 2758.
- [5] K. Parvez, Z. S. Wu, R. J. Li, X. J. Liu, R. Graf, X. L. Feng, K. Mullen, *J. Am. Chem. Soc.* **2014**, 136, 6083.
- [6] K. Parvez, R. J. Li, S. R. Puniredd, Y. Hernandez, F. Hinkel, S. H. Wang, X. L. Feng, K. Mullen, *ACS Nano* **2013**, 7, 3598.
- [7] A. Eckmann, A. Felten, A. Mishchenko, L. Britnell, R. Krupke, K. S. Novoselov, C. Casiraghi, *Nano Lett.* **2012**, 12, 3925.
- [8] E. Bekyarova, M. E. Itkis, P. Ramesh, C. Berger, M. Sprinkle, W. A. de Heer, R. C. Haddon, *J. Am. Chem. Soc.* **2009**, 131, 1336.
- [9] D. Belanger, J. Pinson, *Chem. Soc. Rev.* **2011**, 40, 3995.
- [10] D. A. C. Brownson, D. K. Kampouris, C. E. Banks, *Chem. Soc. Rev. Solid State Commun* **2012**, 41, 6944.



Click here to access/download

Supporting Information

20170922-AM-revision-SI.doc











Click here to access/download
Production Data
Figure4.tif





[Click here to access/download](#)

Production Data
Figure6.tif






Click here to access/download
Production Data
FigureS1.tif



Click here to access/download
Production Data
FigureS10.tif



Click here to access/download
Production Data
FigureS11.tif





Click here to access/download
Production Data
FigureS13.tif














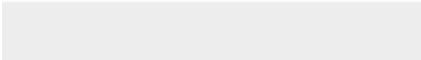

[Click here to access/download](#)

Production Data
FigureS7.tif





Click here to access/download
Production Data
FigureS9.tif





Click here to access/download
Production Data
Short Summary.docx



Click here to access/download
Production Data
Imagefortableofcontents.tif

